NASA/TP–2010–216133



Spacecraft Solar Particle Event (SPE) Shielding:

Shielding Effectiveness as a Function of SPE Model as Determined with the FLUKA Radiation Transport Code

Steve Koontz[1]
William Atwell[2]
Brandon Reddell[1]
Kristina Rojdev[1,3]

[1]*NASA Johnson Space Center, Houston*
[2]*The Boeing Company, Boeing Research & Technology, Houston*
[3]*PhD Student, University of Southern California, Los Angeles*
Johnson Space Center, Houston

National Aeronautics and
Space Administration

Johnson Space Center
Houston, TX 77058

September 2010

THE NASA STI PROGRAM OFFICE . . . IN PROFILE

Since its founding, NASA has been dedicated to the advancement of aeronautics and space science. The NASA Scientific and Technical Information (STI) Program Office plays a key part in helping NASA maintain this important role.

The NASA STI Program Office is operated by Langley Research Center, the lead center for NASA's scientific and technical information. The NASA STI Program Office provides access to the NASA STI Database, the largest collection of aeronautical and space science STI in the world. The Program Office is also NASA's institutional mechanism for disseminating the results of its research and development activities. These results are published by NASA in the NASA STI Report Series, which includes the following report types:

- TECHNICAL PUBLICATION. Reports of completed research or a major significant phase of research that present the results of NASA programs and include extensive data or theoretical analysis. Includes compilations of significant scientific and technical data and information deemed to be of continuing reference value. NASA's counterpart of peer-reviewed formal professional papers but has less stringent limitations on manuscript length and extent of graphic presentations.
- TECHNICAL MEMORANDUM. Scientific and technical findings that are preliminary or of specialized interest, eg, quick release reports, working papers, and bibliographies that contain minimal annotation. Does not contain extensive analysis.
- CONTRACTOR REPORT. Scientific and technical findings by NASA-sponsored contractors and grantees.
- CONFERENCE PUBLICATION. Collected papers from scientific and technical conferences, symposia, seminars, or other meetings sponsored or cosponsored by NASA.
- SPECIAL PUBLICATION. Scientific, technical, or historical information from NASA programs, projects, and mission, often concerned with subjects having substantial public interest.
- TECHNICAL TRANSLATION. English-language translations of foreign scientific and technical material pertinent to NASA's mission.

Specialized services that complement the STI Program Office's diverse offerings include creating custom thesauri, building customized databases, organizing and publishing research results . . . even providing videos.

For more information about the NASA STI Program Office, see the following:

- Access the NASA STI Program Home Page at http://www.sti.nasa.gov
- E-mail your question via the Internet to help@sti.nasa.gov
- Fax your question to the NASA Access Help Desk at (301) 621-0134
- Telephone the NASA Access Help Desk at (301) 621-0390
- Write to:
  NASA Access Help Desk
  NASA Center for AeroSpace Information
  7115 Standard
  Hanover, MD 21076-1320

NASA/TP–2010–216133



Spacecraft Solar Particle Event (SPE) Shielding:

Shielding Effectiveness as a Function of SPE Model as Determined with the FLUKA Radiation Transport Code

Steve Koontz[1]
William Atwell[2]
Brandon Reddell[1]
Kristina Rojdev[1,3]

[1]*NASA Johnson Space Center, Houston*
[2]*The Boeing Company, Boeing Research & Technology, Houston*
[3]*PhD Student, University of Southern California, Los Angeles*
Johnson Space Center, Houston

National Aeronautics and
Space Administration

Johnson Space Center
Houston, TX 77058

September 2010

Available from:

NASA Center for AeroSpace Information
7115 Standard Drive
Hanover, MD 21076-1320
Phone: 301-621-0390 or
Fax: 301-621-0134

National Technical Information Service
5285 Port Royal Road
Springfield, VA 22161
703-605-6000

This report is also available in electronic form at http://ston.jsc.nasa.gov/collections/TRS/

Contents

	Abstract	1
1	Introduction	1
2	Calculating Spacecraft Ionizing Dose and Single-event Rates with FLUKA	2
2.1	Number of proton reaction upsets = [event proton fluence > 50 MeV] × σ(proton > 50 MeV)	3
3.	Solar Particle Event Spectra	4
4.	Results and Discussion – Ionizing Dose and Star Density	7
5.	Results and Discussion – Single-event Environment Rates	18
6.	Summary and Conclusions	19
7.	References	20
	Appendix	22

Figures

1 The concentric spherical shell spacecraft structured used in FLUKA simulations 3
2 A comparison of the Band and Exponential SPE spectra (differential and integral forms) for the July 2000 SPE 5
3 A comparison of the Band and Exponential SPE spectra (differential and integral forms) for the November 2001 SPE 6
4 A comparison of the Band and Exponential SPE spectra (differential and integral forms) for the November 1997 SPE 6
5 A comparison of the Band and Exponential SPE spectra (differential and integral forms) for the October 2003 SPE 7
6 Dose, in cGy (y axis, range 10^{-3} to 10^{5}), to the silicon detector shells as a function of shielding mass in g/cm^2 *aluminum* (x axis, range 0.1 to 1 000) for each of the four particle events considered in this paper 9
7 Dose, in cGy (y axis, range 10^{-3} to 10^{5}), to the silicon detector shells as a function of shielding mass in g/cm^2 *polyethylene* (x axis, range 0.1 to 100) for each of the four particle events considered in this paper 10
8 Dose, in cGy (y axis, range 10^{-3} to 10^{5}), to the silicon detector shells as a function of shielding mass in g/cm^2 *carbon* (x axis, range 0.1 to 10^{3}) for each of the four particle events considered in this paper 11
9 Dose, in cGy (y axis, range 10^{-3} to 10^{5}), to the silicon detector shells as a function of shielding mass in g/cm^2 *titanium* (x axis, range 0.1 to 1 000) for each of the four particle events considered in this paper 12
10 Proton star density, in number per cc (y axis, range 0.1 to 10^{5}), to the silicon detector shells as a function of shielding mass in g/cm^2 *aluminum* (x axis, range 0.1 to 10^{3}) for each of the four particle events considered in this paper 14
11 Proton star density, in number per cc (y axis, range 0.1 to 10^{5}), to the silicon detector shells as a function of shielding mass in g/cm^2 *polyethylene* (x axis, range 0.1 to 100) for each of the four particle events considered in this paper 15
12 Proton star density, in number per cc (y axis, range 0.1 to 10^{5}), to the silicon detector shells as a function of shielding mass in g/cm^2 *carbon* (x axis, range 0.1 to 100) for each of the four particle events considered in this paper 16
13 Proton star density, in number per cc (y axis, range 0.1 to 10^{5}), to the silicon detector shells as a function of shielding mass in g/cm^2 *titanium* (x axis, range 0.1 to 1 000) for each of the four particle events considered in this paper 17
14 Proton, neutron, and pion star density, in number per cc (y axis, range 10 to 10^{8}), to the silicon detector shells as a function of aluminum or polyethylene shielding mass in g/cm^2 18

App-1 In 1a and 1b above, HZETRN two-dimensional calculations of dose as a function of depth are compared for the Band and Exponential forms of the event spectra; in 1c and 1d above, three-dimensional FLUKA and two-dimensional HZETRN calculations of dose vs. depth are compared 22

Tables

1 Shielding mass or thickness exterior to each silicon detector shell 3
2 Solar particle event parameters 4
3 A comparison of observed in-flight SPE SEU counts with estimates of SPE SEU counts calculated with FLUKA radiation transport code 19

Acronyms

AU	astronomical unit
DRAM	dynamic random access memory
DSP	digital signal processor
EMU	extravehicular mobility unit
ESP	energetic solar particle event
EVA	extravehicular activity
FLUKA	FLUktuierende KAskade
GLE	ground-level event
GEO	geosynchronous Earth orbit
ICRU	International Commission on Radiation Units
LET	linear energy transfer
SEE	single-event environment
SEU	single-event upset
SPE	solar particle event
SRAM	standard random access memory
SSR	solid-state recorder
TID	total ionizing dose

Abstract

In the following paper, we report the results of modeling and simulation studies in which the radiation transport code FLUKA (FLUktuierende KAskade) is used to determine the changes in total ionizing dose (TID) and single-event effect (SEE) environments behind aluminum, polyethylene, carbon, and titanium shielding masses when the assumed form (ie, Band or Exponential) of the solar particle event (SPE) kinetic energy spectra is changed. FLUKA simulations have fully three spatial dimensions with an isotropic particle flux incident on a concentric spherical shell shielding mass and detector structure. The effects are reported of both energetic primary protons penetrating the shield mass and secondary particle showers caused by energetic primary protons colliding with shielding mass nuclei. SPE heavy ion spectra are not addressed. Our results, in agreement with previous studies, show that use of the Exponential form of the event spectra can seriously underestimate spacecraft SPE TID and single-event environments in some, but not all, shielding mass cases.

1. Introduction

The design and verification of any spacecraft, piloted or unpiloted, required to function in a solar particle event (SPE) environment must begin with the selection of a reasonable worst-case SPE design and verification environment[1], a task complicated by the extreme variability of SPEs[2]. Another difficulty is posed by the fact that event kinetic energy spectra are measured by spacecraft instruments over a limited range of particle kinetic energies, and the full spectrum is only obtained by modeling and extrapolation[3-6]. Radiation transport and modeling studies have shown that the single-event and total ionizing dose (TID) environments behind spacecraft shielding mass depend strongly on the assumed form (ie, Band or Exponential) of the SPE kinetic energy spectra[3–6].

In this paper, we report the results of modeling and simulation studies in which the radiation transport code FLUKA (FLUktuierende KAskade) is used to determine the changes in both the TID and SEE environments behind various thicknesses of aluminum, polyethylene, carbon, and titanium, shielding when the assumed form (ie, Band or Exponential) of the SPE kinetic energy spectra is changed[4-6]. FLUKA is a fully integrated and extensively verified Monte Carlo simulation package for the interaction and transport of high-energy particles and nuclei in matter[7-9].

The SPE spectra investigated are taken from four specific SPEs that produced ground-level events (GLEs) during solar cycle 23 (1997–2008)[6]. GLEs are produced by highly energetic solar particle events (ESP), ie, those that contain significant fluences of 700 MeV to 10 GeV protons. High-energy protons interact with Earth's atmosphere via nuclear reaction to produce secondary particles, some of which are neutrons that can be detected at the Earth's surface by the global neutron monitor network[10,11]. GLEs are one part of the overall SPE resulting from a particular solar flare or coronal mass ejection event on the Sun. The ESP part of the particle event, detected by spacecraft, is often associated with the arrival of a "shock front" at Earth[6] some hours after the arrival of the GLE.

Highly energetic SPEs are implicated in increased rates of spacecraft anomalies and spacecraft failures[12–14]. The specific SPEs used in this analysis are those of: 1) November 6, 1997 – GLE only; 2) July 14-15, 2000 – GLE from the 14th plus ESP from the 15th; 3) November 4-6, 2001 – GLE and ESP from the 4th; and 4) October 28-29, 2003 – GLE and ESP from the 28th plus GLE from the 29th. The corresponding Band and Exponential spectra used in this paper are like those previously reported[4-6].

The effects are reported of both energetic primary protons penetrating spacecraft shielding mass and secondary particle showers caused by energetic primary protons colliding with shielding mass nuclei. The SPE spectra impinging on a particular spacecraft will depend on spacecraft location and trajectory[14]. SPE spectra inside planetary magnetospheres are not the same as those observed in interplanetary space. The SPE spectra used in the modeling and simulation study reported here are interplanetary free-space spectra; the results are applicable only at or beyond geosynchronous Earth orbit (GEO) and only at distances on the order of 1 astronomical unit (AU) from the sun. SPE heavy ion spectra and their effects on spacecraft ionizing dose and single-event rates are not directly addressed in this paper[15].

2. Calculating Spacecraft Ionizing Dose and Single-event Rates with FLUKA

FLUKA is a fully integrated Monte Carlo simulation package for the interaction and transport of high-energy particles in matter, including explicit physics-based hadron-nucleus and nucleus-nucleus collisions, with fully developed and complete secondary particle shower production[7-9]. The code is widely and successfully used in particle physics, high-energy experimental physics and engineering, shielding, detector and telescope design, cosmic-ray studies, radiation dosimetry, medical physics, and radiobiology because its precision and accuracy has been exhaustively validated[16-18].

The highest priority in the design and development of FLUKA has always been the implementation and improvement of sound and modern physical models. Microscopic models are adopted whenever possible, with consistency ensured among all reaction steps and/or reaction types. Conservation laws are enforced at each step, and results are checked against experimental data at the single-interaction level. As a result, final predictions are obtained with a minimal set of free parameters for all energy/target/projectile combinations. Therefore, results in complex cases, as well as properties and scaling laws, arise naturally from the underlying physical models. Predictivity is provided where no experimental data are directly available, and correlations within interactions and among shower components are preserved.

FLUKA simulations were conducted on a generic concentric spherical shell "spacecraft" geometry with thin layers (100 microns) of silicon "scoring" detectors between layers of aluminum (or other) shielding masses. The concentric spherical shell geometry is shown in figure 1. FLUKA randomly samples the natural particle kinetic energy spectra appropriate to the specific flight environment to specify particle identity and particle kinetic energy. The selected particles are randomly directed into the spherical shell structure from the outside so as to simulate an isotropic (ICRU [International Commission on Radiation Units] definition) particle flux incident on the "spacecraft."

Each silicon scoring detector shell has a well-defined shielding mass distribution function that is calculated looking outward from the scoring detector shell. The millions of randomly directed particles FLUKA sends into the target sphere during execution of the program accurately sample that shielding mass distribution function. The minimum shielding mass, measured along the spherical target radius and exterior to each silicon detector shell, is shown in Table 1 along with the distance in centimeters from each detector shell to the exterior surface of the concentric spherical target "spacecraft." The interior of the sphere is treated as a perfect particle absorber.

FLUKA reports results based on the isotropic flux to an entire detector shell, not on results based on a limited area of the shell. For each particle fired into the "spacecraft," FLUKA calculates the following through the thickness of the target structure: 1) energy loss (linear energy transfer [LET]) of primary particles, 2) nuclear reactions and reaction products (secondary particle showers), and 3) energy loss and further nuclear reactions of secondary particles.

The FLUKA "SCORE" output tables[19] report total energy deposition, a number proportional to TID, by all primary and secondary particles in each silicon detector shell as well as the number of inelastic nuclear interactions (nuclear reactions or "stars"[*]) produced by > 50 MeV protons, neutrons, and pions. Hadrons < 50 MeV are not scored as stars but do contribute to TID. Because FLUKA is a Monte Carlo code, results will vary from run to run as the random number seed is changed. It follows that only the average of two or more FLUKA runs should be compared with the results of deterministic codes like HZETRN[20]. The general characteristics of HZETRN were communicated to author 2in a conversation with Dr Martha S. Clowdsley, NASA Langley Research Center in 2007.

Spacecraft proton SEE rates for each particle event are *estimated* from the total > 50 MeV proton fluence for each silicon detector shell. The contribution to the single-event rate from proton nuclear reactions for each silicon detector shell is estimated by multiplying the >50 MeV proton event fluence for each silicon shell by the saturated proton cross section for the component of interest as determined by ground-based heavy ion testing combined with the Petersen-Barak method[21]. The total > 50 MeV proton fluence for each detector shell is calculated from the

[*]A star is a nuclear reaction event in a solid target material caused by the collision of an energetic hadron (proton, neutron, or pion) with a target material nucleus.

detector shell proton star density and the inelastic collision length of protons[22]. Finally, SPE proton-induced single event upsets are estimated using the equation below.

Number of proton reaction upsets = [event proton fluence > 50 MeV] × σ(proton > 50 MeV)

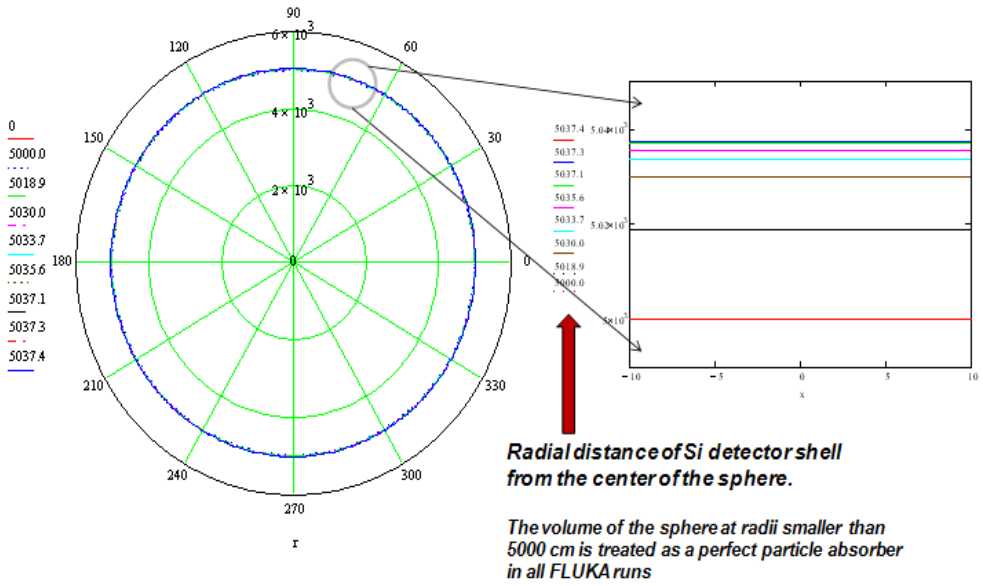


Figure 1. The concentric spherical shell spacecraft structure used in FLUKA simulations.

Table 1. Shielding mass or thickness exterior to each silicon detector shell

Concentric Sphere Shield Thickness (g/cm^2)	SiDet1	SiDet1	SiDet1	SiDet1	SiDet1	SiDet1	SiDet1	SiDet1
Polyethylene	0.036	0.175	0.380	1.854	3.677	7.316	18.213	36.719
Carbon	0.074	0.357	0.775	3.783	7.504	14.93	37.169	74.963
Aluminum	0.100	0.482	1.046	5.107	10.131	20.155	50.178	101.164
Titanium	0.167	0.803	1.743	8.512	16.885	33.592	83.603	168.607
Shield Geometric Thickness (cm)	0.056	0.300	0.593	2.926	5.778	11.519	28.704	57.852

SEE rate calculations (estimates) were made for three different spacecraft, flying at GEO or beyond, for which SPE SEE rates have been measured in-flight. The three spacecraft/electronic component combinations are: 1) Cassini[23] SSR [solid-state recorder] DRAM [dynamic random access memory], 2) SOHO[24] SSR DRAM, and, 3) Thuraya[25] DSP [digital signal processor] SRAM [static random access memory]. Cassini was exposed to the November 6, 1997 SPE shortly after launch. SOHO was exposed to both the November 6, 1997 and the July 14-15, 2000 SPEs. Thuraya was exposed to both the November 4-6, 2001 and the October 28-29, 2003 events. All three spacecraft were located at approximately 1 AU from the sun and are either in geosynchronous orbit or beyond but still very close to 1 AU

from the sun. All three spacecraft reported significant increases in single-event upset (SEU) rates during the SPEs and much lower background rates, caused by galactic cosmic rays, before and after the events.

SPE proton-induced SEU rate calculations are very sensitive to assumptions concerning the spacecraft shielding mass. Unfortunately, detailed shielding mass distribution functions are not available for the subject spacecraft. So, shielding mass is estimated as follows: The minimum shielding mass estimate provided in Refs. 23-25 is configured as a hollow sphere, and the SEE-sensitive devices are placed on the inner wall of the sphere. The median shielding mass for each device is then found by multiplying the minimum shielding mass by 1.56 to obtain the median shielding mass at that location. The interior of the sphere, containing the rest of the spacecraft mass, is treated as opaque to the vast majority of the event protons so that only protons entering the device through the spherical shell exterior to the device are effective in causing upsets. The estimated median shielding mass for each spacecraft/electronic component combinations is as follows: 1) Cassini SSR DRAM, 7 g/cm^2; 2) SOHO SSR DRAM, 2 g/cm^2; and 3) Thuraya DSP SRAM, 2 g/cm^2. Spacecraft shielding mass is assumed to be aluminum.

The proton star density from the FLUKA simulations corresponding to the median shielding mass is then used to calculate the >50 MeV proton event fluence. One half of the event proton fluence so calculated is used to calculate the estimated event SEU rate. One half of the event fluence is the appropriate fluence to use in the assumed spacecraft geometry because particle flux is incident from 4π steradians on the entire surface of the concentric sphere structure used in the FLUKA simulations and FLUKA reports results for entire spherical regions, eg, detector shells. In contrast, the particle flux to *any single point* on an opaque sphere is incident from only 2π steradians.

The spacecraft components listed above are not subject to SEE effects resulting from direct ionization by the energetic protons passing through the components because the maximum proton LET [linear energy transfer] is well below the device LET threshold in all cases. Instead, SEE effects result from both the nuclear reactions between primary and secondary energetic protons (and other hadrons) and the silicon nuclei in the electronic devices that produce high-LET secondary particles internal to the devices.

SPEs also contain a not insignificant heavy ion (eg, carbon, oxygen, and iron) content that can cause SEE events in microelectronic devices by direct ionization[15], although the magnitude of the contribution varies from spacecraft to spacecraft and event to event[25,26]. The expected contribution of heavy ions to the event SEU observations for the spacecraft considered here are examined below in the results and discussion section of this paper.

3. Solar Particle Event Spectra

For the SPEs considered in this paper, the full event was taken into account; ie, the summation of the semi-empirical exponential spectra observed by satellite (ESP) and the enhanced GLE, when available and that may have occurred on the same day or the day before or after. The GLE is a higher-energy part of the spectrum (> 700 MeV) associated with the SPEs that are detected by high-latitude neutron-monitoring stations. These neutrons are a result of the secondary particle shower created when the high-energy protons interact with the Earth's atmosphere[6,10,11]. The spectra used in this paper were derived using the parameters shown in Table 2.

Table 2. Solar particle event parameters

Event Start Date					
Nov. 6, 1997	GLE	8.15E+8	0.284	5.38	116
July 14, 2000	GLE	2.94E+9	0.506	7.46	123
July 15, 2000	ESP	6.01E+7	3.235	7.85	226
Nov. 4, 2001	GLE	2.14E+9	0.242	6.67	93
Nov. 4, 2001	ESP	4.78E+8	2.363	11.2	129
Oct. 28, 2003	GLE	8.44E+9	0.0086	6.48	89
Oct. 28, 2003	ESP	1.12E+8	2.812	8.92	171
Oct. 29, 2003	GLE	7.62E+7	2.004	6.86	206

The Band integral spectra for the GLEs were computed using the above parameters and the following expressions[6]:

$$J(>R) = J_0 R^{-\gamma_1} \exp\left(-\frac{R}{R_0}\right), \text{ for } R \le (\gamma_2 - \gamma_1) R_0.$$

$$J(>R) = J_0 R^{-\gamma_2} \left\{\left[(\gamma_2 - \gamma_1) R_0\right]^{(\gamma_2 - \gamma_1)} \exp(\gamma_1 - \gamma_2)\right\}, \text{ for } R \ge (\gamma_2 - \gamma_1) R_0.$$

As mentioned above, for each event the integral spectra from all associated GLEs and ESPs were summed to get a total integral spectrum for that event. The total differential spectrum was created by differentiating the integral spectra with respect to particle kinetic energy.

For the Exponential spectra, only the J_0 parameter is used from Table 2. The expression to derive the Exponential spectra is as follows:

$$J(>R) = J_0 \exp\left(-\frac{R}{R_0}\right).$$

The total Exponential spectrum for each event was created in a similar manner to the Band total integral spectrum. However, for this spectrum, the total differential spectrum was created from a code that maintains the Exponential functional form in rigidity based on the total integral (> 30 MeV) and (>100 MeV) values. Because the exponential fluence drops off rapidly, only energies up to 1 000 MeV were considered in this paper. Contributions to dose and SEE are negligible at these higher energies.

The integral form of the Band and Exponential SPE kinetic energy spectra are compared in figures 2 through 5 for each of the four SPEs considered in this paper.

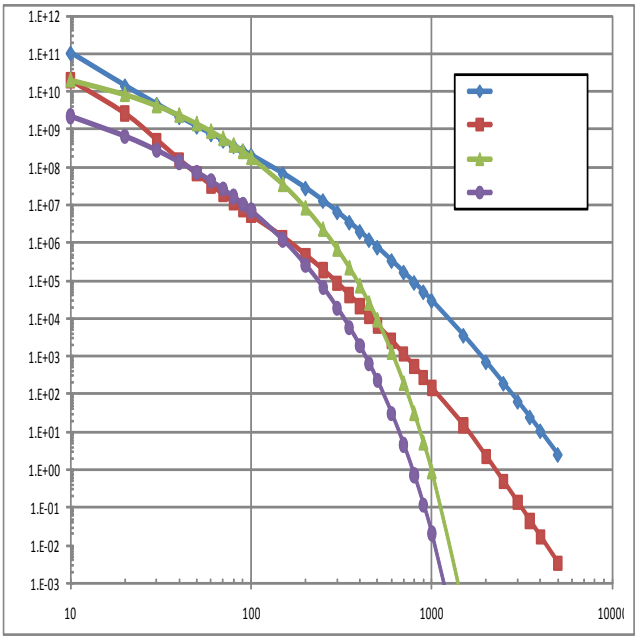


Figure 2. A comparison of the Band and Exponential SPE spectra (differential and integral forms) for the July 2000 SPE. X axis = particle kinetic energy in MeV; Y axis = protons/cm^2 for integral spectra and protons/(cm^2 MeV) for differential spectra.

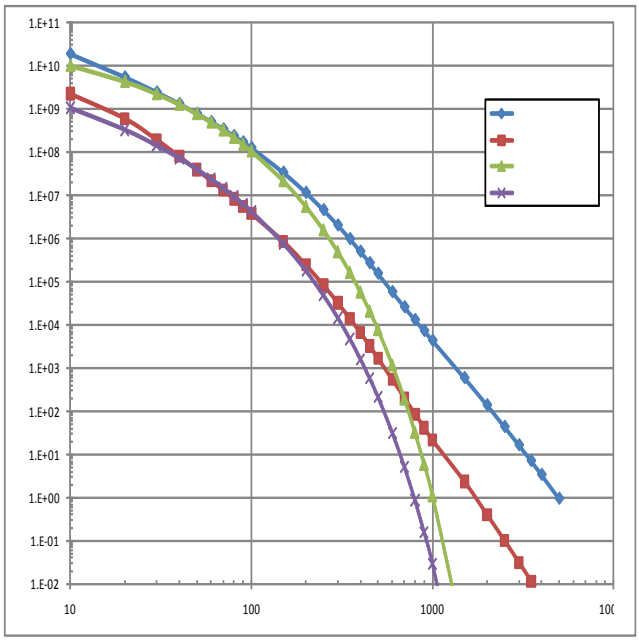


Figure 3. A comparison of the Band and Exponential SPE spectra (differential and integral forms) for the November 2001 SPE. X axis = particle kinetic energy in MeV; Y axis = protons/cm^2 for integral spectra and protons/(cm^2 MeV) for differential spectra.

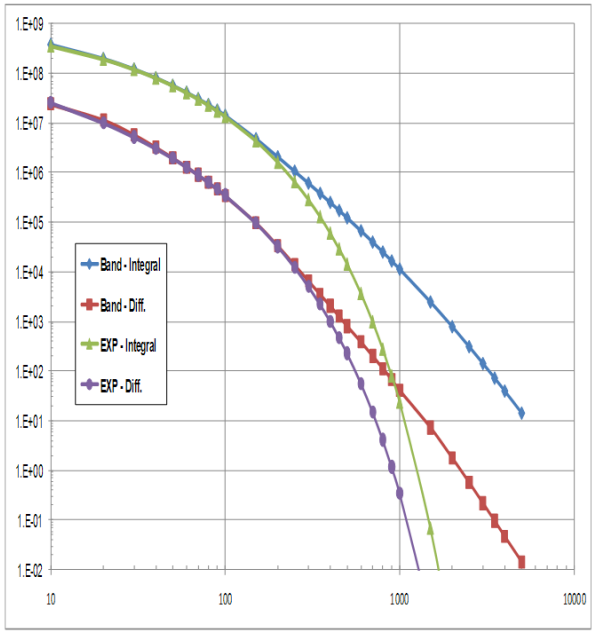


Figure 4. A comparison of the Band and Exponential SPE spectra (differential and integral forms) for the November 1997 SPE. X axis = particle kinetic energy in MeV; Y axis = protons/cm^2 for integral spectra and protons/(cm^2 MeV) for differential spectra.

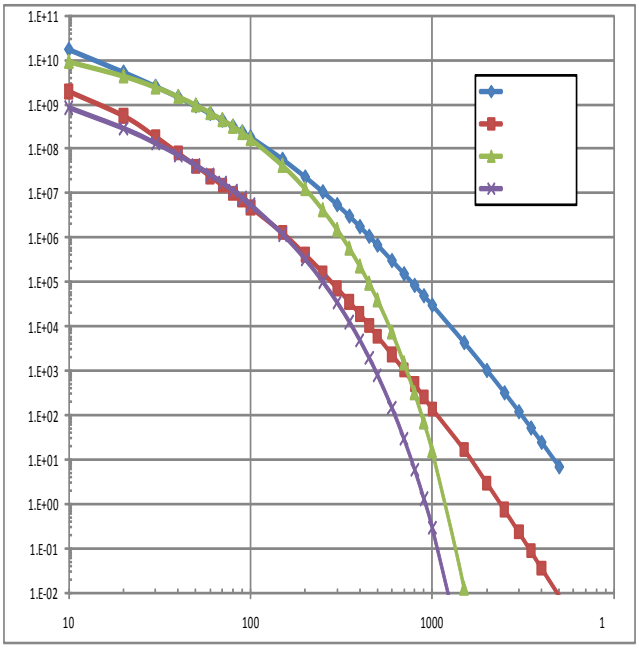


Figure 5. A comparison of the Band and Exponential SPE spectra (differential and integral forms) for the October 2003 SPE. X axis = particle kinetic energy in MeV; Y axis = protons/cm^2 for integral spectra and protons/(cm^2 MeV) for differential spectra.

4. Results and Discussion – Ionizing Dose and Star Density

The results of FLUKA calculations of SPE TID, expressed in cGy, as a function of shielding mass, expressed in g/cm^2, are shown in figures 6 through 9 as is the ratio (Band dose)/(Exponential dose). Note that in all the figures, the curve connecting the calculated data points is merely a guide for the eye, not a fitting function. For TID, the statistical run-to-run variation is on the order of 10% of the indicated value or less, so error bars are not plotted. Results are plotted on log-log axes, and data ranges for the x and y axes are indicated in the figure captions. With the exception of the November 1997 event, the TID produced by the Band spectra exceeded that produced by Exponential spectra only at the lowest and highest shielding masses. In the middle shielding mass range, the Band TID and Exponential TID are very nearly the same. Band TID is significantly greater than Exponential TID only at high shielding mass in the November 1997 event. For all particle event shielding mass combinations, Band TID and Exponential TID are very nearly equal in the shielding mass range of 1 to 10 g/cm^2.

The comparison of Band and Exponential TID as a function of shielding mass (shown in figs. 6-9) is reminiscent of the comparison of the Band and Exponential spectra shown in figures 2 through 5. The Band and Exponential spectra are very nearly identical between 30 and 200 MeV, while diverging only below 30 and above 200 MeV. The relationship between proton kinetic energy and range in solids suggests that the low-energy protons are the most important contributors to dose at low shielding mass while the highest-energy protons are the most important contributors to dose at the highest shielding mass. Protons between and 200 MeV are the most important contributors to dose in the middle shielding mass range.

With the exception of the November 1997 event and for all shielding materials studied, the shielding mass needed to reduce the event ionizing dose to 1 cGy or less is always greater than 10 but less than 50 g/cm^2. The usual atomic number dependence of shielding effectiveness is observed. For example, in the July 2000 event Band plots the shielding mass, measured along the sphere radius needed to reduce the event ionizing dose to 1 cGy or less in the concentric sphere configuration, is 30 g/cm^2 polyethylene, 37 g/cm^2 carbon, 40 g/cm^2 aluminum, and 43 g/cm^2 titanium. Using the Exponential July 2000 event spectrum, the shielding mass needed to reduce the event ionizing dose to 1 cGy or less is 22 g/cm^2 polyethylene, 25 g/cm^2 carbon, 29 g/cm^2 aluminum, and 32 g/cm^2 titanium. Use of the Band spectra

for design and verification will lead to a heavier spacecraft, but this additional weight may be necessary to assure meeting some event TID requirements. The weight impact can be minimized by selecting materials and spacecraft configurations with optimum radiation shielding performance.

The choice of Band or Exponential event spectra can significantly affect spacecraft mass for allowable doses of 1 cGy or less. However, as shown in figures 6 through 9, for allowable doses between 10 and 100 cGy the difference between Band and Exponential TID is negligible. If either the Exponential or Band spectra are selected in combination with an allowable event TID between 10 and 100 cGy, the spacecraft should meet allowable dose design requirements during flight operations.

Event TIDs between 10 and 100 cGy correspond to shielding masses between 1 and 10 g/cm^2, so there is no significant difference in the TID produced by the Band or Exponential event spectra over the subject shielding mass range. For spacecraft having shielding mass between 1 and 10 g/cm^2, the choice of Exponential or Band event spectra for design and verification is of no special importance in all cases studied.

The choice of Band or Exponential spectra can be important at shielding mass values below 1 g/cm^2 where the event TID can exceed 10^4 cGy and the Band TID can be an order of magnitude greater than the Exponential TID. With the exception of the November 1997 event, Band TID is between two and 10 times Exponential TID in all cases studied over the subject shielding mass range. Selection of the Exponential spectra for design and verification can lead to unacceptable hardware degradation during SPEs and may even impact crew health if extravehicular mobility units (EMUs; aka spacesuits) do not provide adequate protection to limit dose during emergency extravehicular activity (EVA; aka spacewalk) termination following an SPE event warning.

The general features of the dose depth curves shown in figures 6 through 9 are also visible in two-dimensional deterministic simulations executed with the HZETRN [a galactic cosmic ray transport code developed at NASA Langley Research Center] on slab targets. As shown in the Appendix, the features of the dose depth curve in figures 6 through 9 are not the result of unexpected three-dimensional geometric effects.

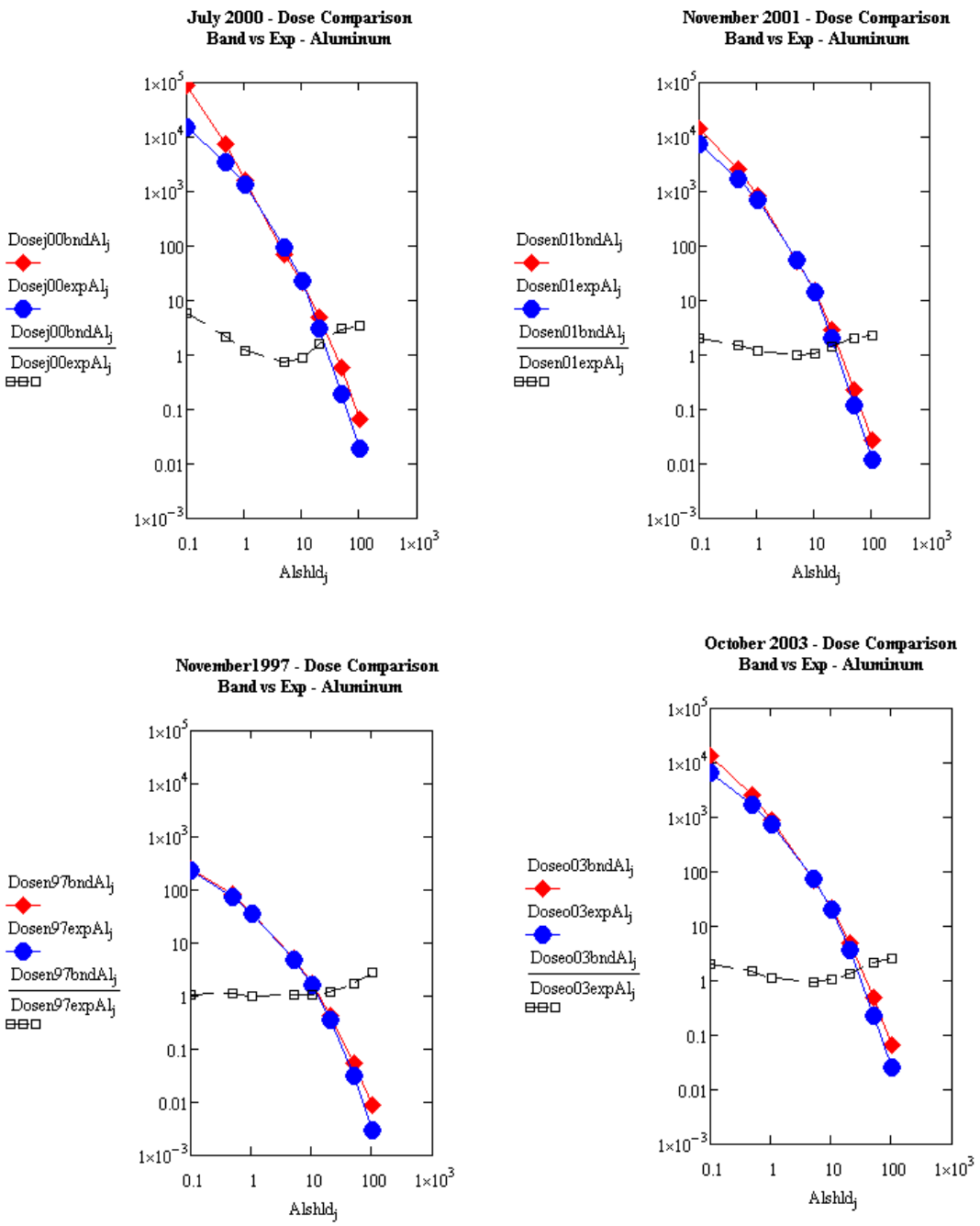


Figure 6. Dose, in cGy (y axis, range 10^{-3} to 10^{5}), to the silicon detector shells as a function of shielding mass in g/cm^2 *aluminum* (x axis, range 0.1 to 1 000) for each of the four particle events considered in this paper. Event dose resulting from Band (◆) and Exponential (●) event spectra is plotted as is the ratio [Band dose]/[Exponential dose] (□).

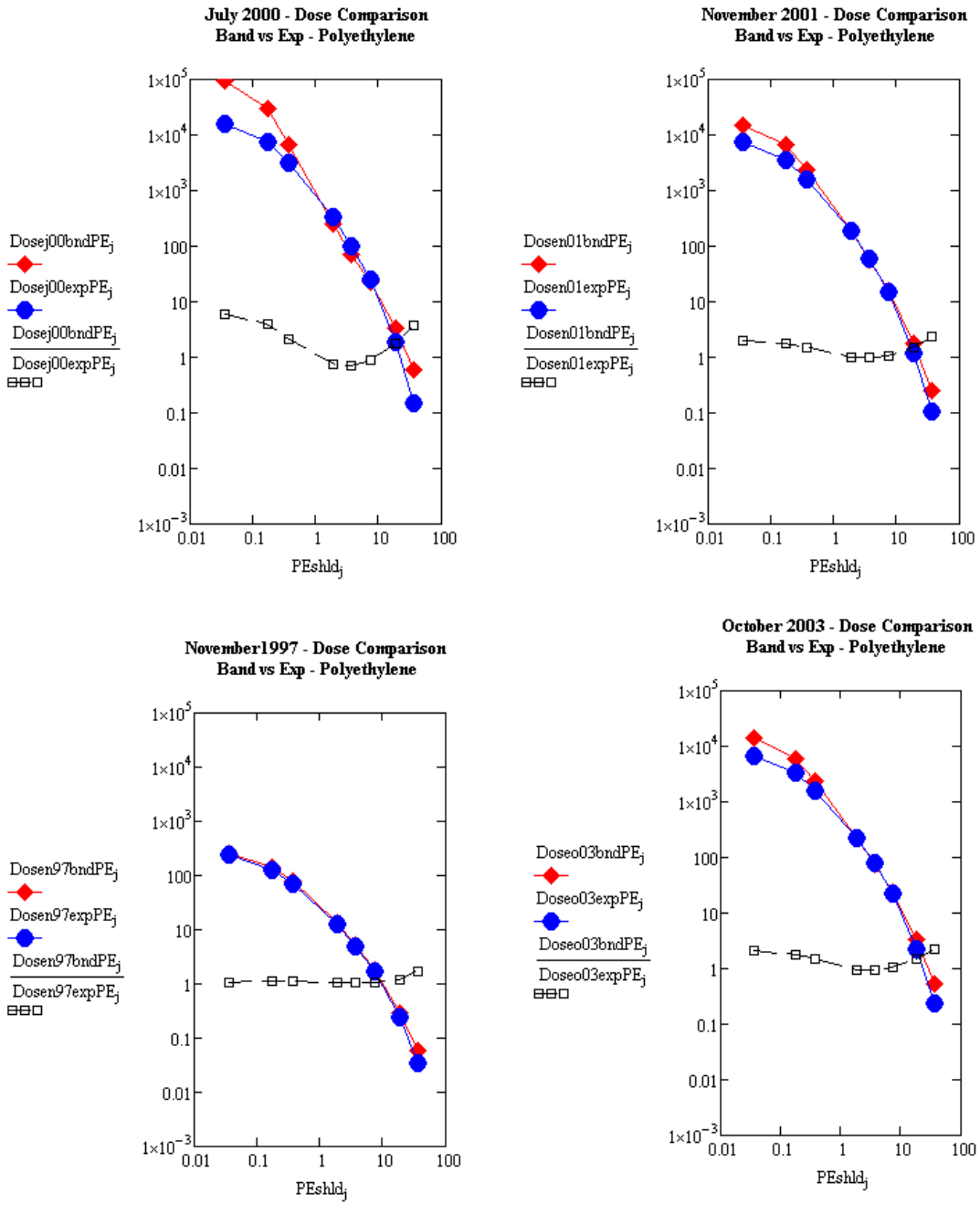


Figure 7. Dose, in cGy (y axis, range 10^{-3} to 10^{5}), to the silicon detector shells as a function of shielding mass in g/cm^2 *polyethylene* (x axis, range 0.1 to 100) for each of the four particle events considered in this paper. Event dose resulting from Band (◆) and Exponential (●) event spectra is plotted as is the ratio [Band dose]/[Exponential dose] (□).

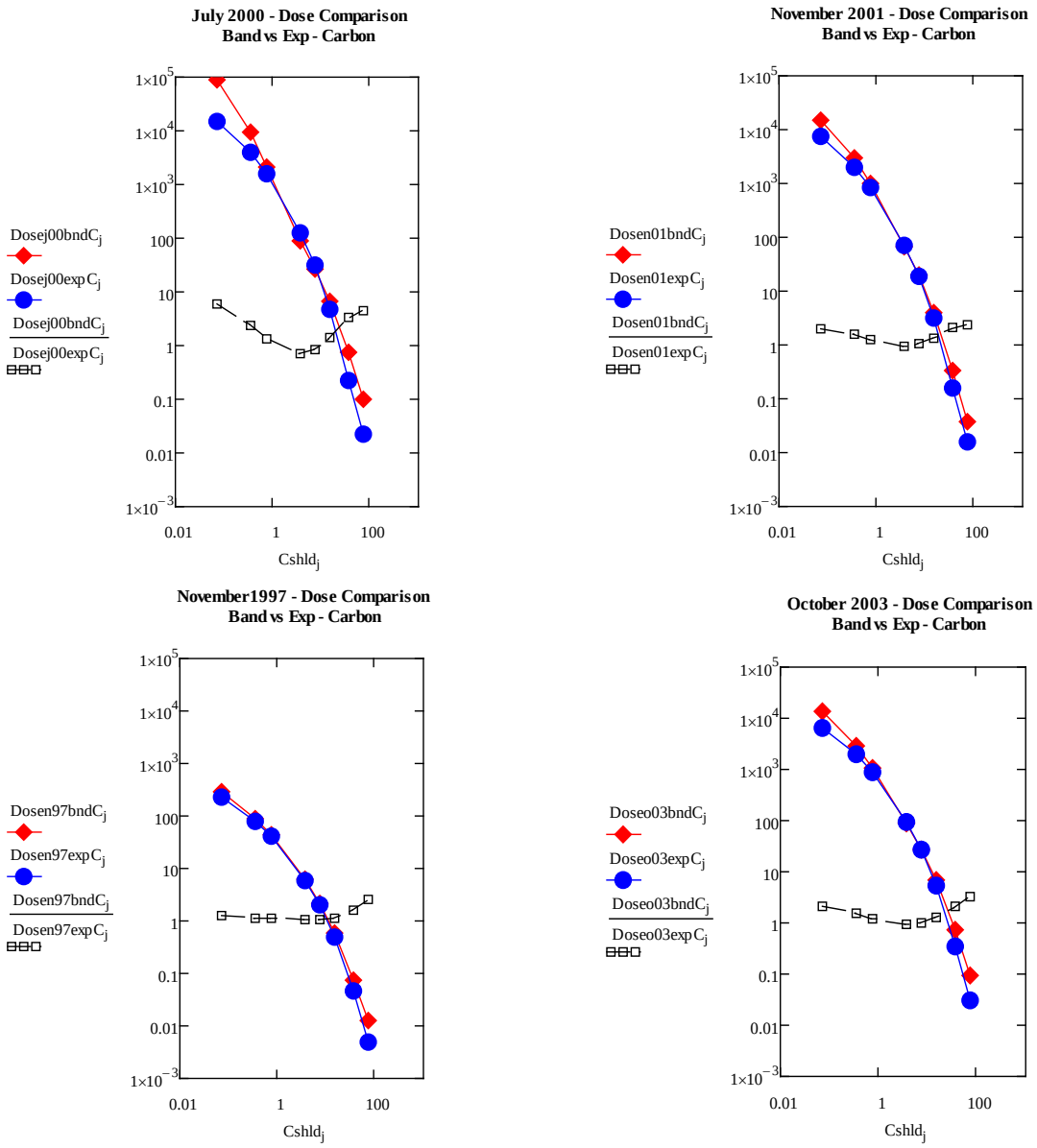


Figure 8. Dose, in cGy (y axis, range 10^{-3} to 10^{5}), to the silicon detector shells as a function of shielding mass in g/cm^2 *carbon* (x axis, range 0.1 to 10^{3}) for each of the four particle events considered in this paper. Event dose resulting from Band (◆) and Exponential (●) event spectra is plotted as is the ratio [Band dose]/[Exponential dose] (□).

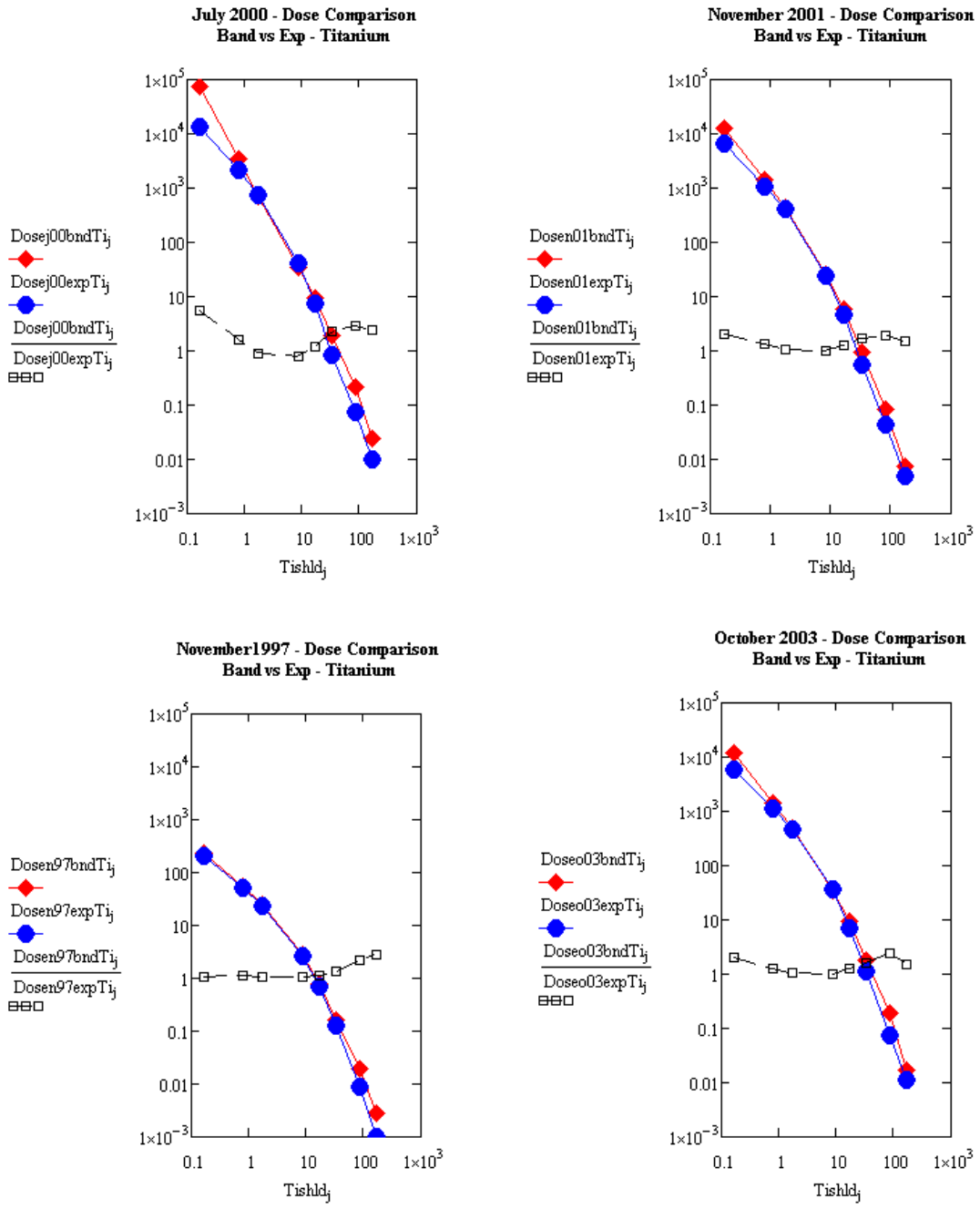


Figure 9. Dose, in cGy (y axis, range 10^{-3} to 10^{5}), to the silicon detector shells as a function of shielding mass in g/cm^2 *titanium* (x axis, range 0.1 to 1 000) for each of the four particle events considered in this paper. Event dose resulting from Band (◆) and Exponential (●) event spectra is plotted as is the ratio [Band dose]/[Exponential dose] (□).

The production of stars, occurring at particle kinetic energy greater than 50 MeV for protons, neutrons, and pions, was dominated by protons for all shielding material SPE combinations studied. The results of FLUKA calculations of proton star density in the silicon detector shells, expressed as stars per cc, are shown in figures 10 through 13 as a function of shielding mass, expressed in g/cm^2 measured along the sphere radius. For proton star production, the statistical run-to-run variation is on the order of 10% of the indicated value or less for shielding masses less than 20 g/cm^2, so error bars are not plotted. Results are plotted on log-log axes, and the data ranges for the x and y axes are indicated in the figure captions

The Band and Exponential spectra are essentially the same for proton kinetic energies between 30 and 200 MeV, and the comparison of Band and Exponential star densities reflect this fact. The Band and Exponential proton star density plots, which are essentially the same at low shielding mass, only diverge for a shielding mass greater than 10 g/cm^2. The ratio (Band star density)/(Exponential star density) is close to 1 below 10 g/cm^2, and can increase to between 2 and 10 at greater shielding mass values. Band and Exponential proton star densities are the same at lower shielding masses because protons having < 50 MeV kinetic energy do not contribute to the star score, yet can be an improtant part of the primary SPE spectrum.

The shielding materials studied exhibit a different order of effectiveness from those observed for ionizing dose. Using the July 2000 SPE Band spectra as an example again, the shielding mass needed to reduce the proton star density to 10^5 stars/cm^3 is 30 g/cm^2 polyethylene, 32 g/cm^2 carbon, 30 g/cm^2 aluminum, and 50 g/cm^2 titanium. Using the July 2000 SPE Exponential SPE band spectra, the shielding mass needed to reduce the proton star density to 10^5 stars/cm^3 is 23 g/cm^2 polyethylene, 24 g/cm^2 carbon, 22 g/cm^2 aluminum, and 32 g/cm^2 titanium.

If maintaining the proton star density (for proton kinetic energies > 50 MeV) during an SPE is a design and verification objective, the selection of the Band or Exponential design environments can lead to substantial differences in spacecraft weight. Picking the Exponential environment may lead to a failure to meet requirements during flight operations.

Neutron and pion star densities, as expected for the relatively small number of particles produced, displayed considerable run-to-run statistical variability; so the results are accurate only to the nearest order of magnitude. Unlike proton stars or ionizing dose, the neutron and pion star density showed little variation with shielding mass. Neutron star densities were between 10^5 and 10^6 stars /cm^3 for higher fluence events and between 10^4 and 10^5 stars/cm^3 for the lower-fluence November 1997 event.

Proton, neutron, and pion star density is shown as a function of aluminum and polyethylene shielding mass for the November 2001 SPE (Band and Exponential spectra) in figure 14. Figure 14 is representative of all SPE event spectra shielding mass combinations. The most immediately obvious difference between the Band and Exponential spectra plots in figure 14 is the essential absence of pion stars in the Exponential case, a not unexpected result given the kinetic energy threshold for pion production. The single pion point in the polyethylene exponential spectra is most probably a statistical fluke (ie, low probability event). The Exponential spectra pion star density was zero for all other shielding mass event combinations.

Despite the relatively large statistical uncertainty on the neutron and pion data, some general trends are apparent. First, the neutron and pion star yields are not significantly higher for the Band than for the Exponential spectra. Second, the number of neutron and pion stars increases to a shallow maximum at or around 10 g/cm^2 before decreasing again at greater shielding mass values. Third and finally, as compared to proton stars, neutron and pion star density shows relatively weak dependence on shielding mass, generally varying by less than an order of magnitude across the entire shielding mass range. At the highest shielding mass values, the neutron star density can be larger than the proton star density.

Star density for > 50 MeV hadronic particles is of interest because it can be used to calculate the corresponding particle flux and fluence at different shielding depths using the particle inelastic interaction collision length[22]. Star density is also directly related to the SEU rate caused by hadronic interactions in or near electronic device sensitive volumes. Proton-driven single-event rates for various spacecraft are predicted using this approach in the next section of this paper for comparison with observed in-flight rates.

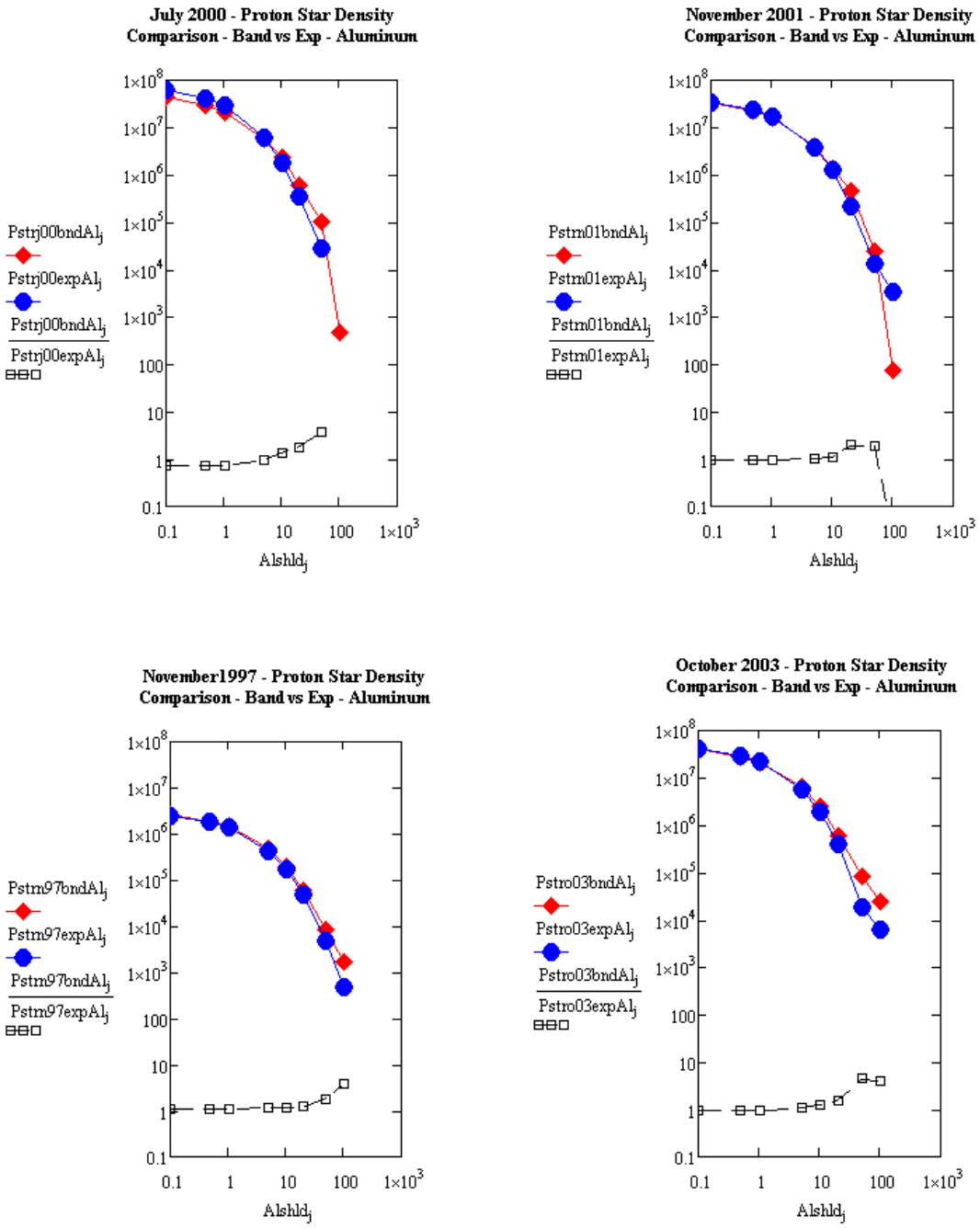


Figure 10. Proton star density, in number per cc (y axis, range 0.1 to 10^5), to the silicon detector shells as a function of shielding mass in g/cm^2 *aluminum* (x axis, range 0.1 to 10^3) for each of the four particle events considered in this paper. Event star density resulting from Band (◆) and Exponential (●) event spectra is plotted as is the ratio [Band star density]/[Exponential star density] (□).

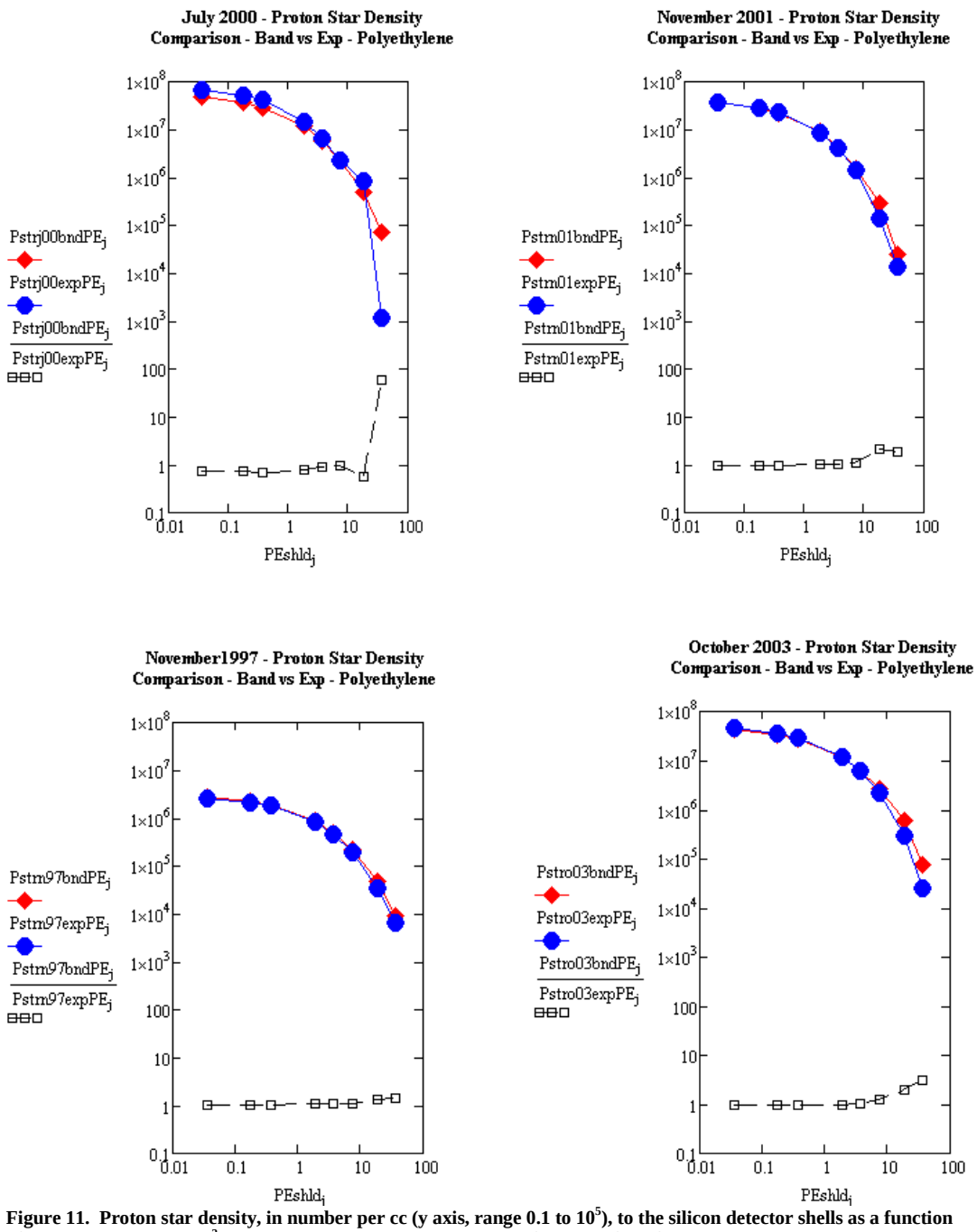


Figure 11. Proton star density, in number per cc (y axis, range 0.1 to 10^5), to the silicon detector shells as a function of shielding mass in g/cm^2 *polyethylene* (x axis, range 0.1 to 100) for each of the four particle events considered in this paper. Event star density resulting from Band (◆) and Exponential (●) event spectra is plotted as is the ratio [Band star density]/[Exponential star density] (□).

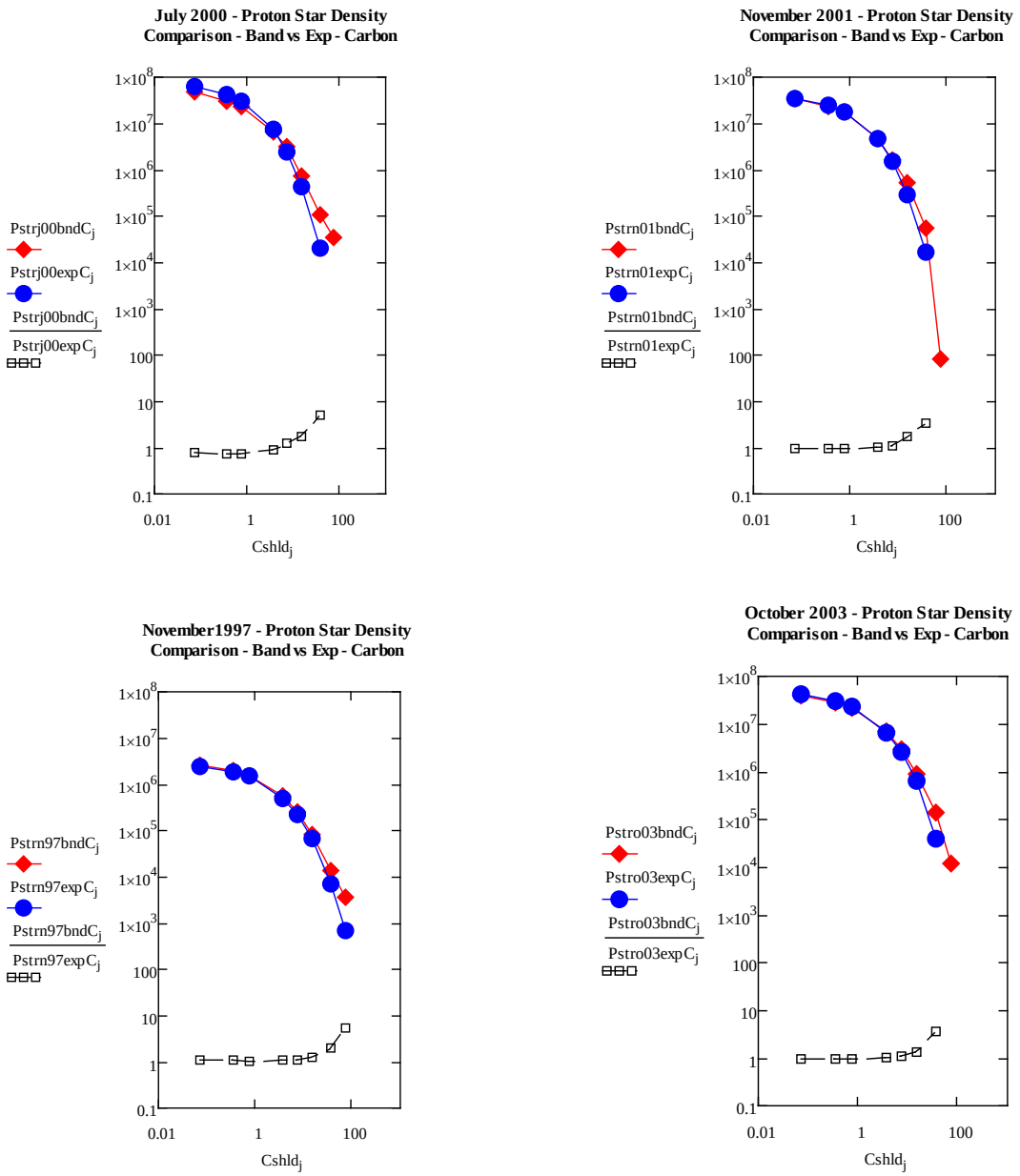


Figure 12. Proton star density, in number per cc (y axis, range 0.1 to 10^5), to the silicon detector shells as a function of shielding mass in g/cm^2 *carbon* (x axis, range 0.1 to 100) for each of the four particle events considered in this paper. Event star density resulting from Band (◆) and Exponential (●) event spectra is plotted as is the ratio [Band star density]/[Exponential star density] (□).

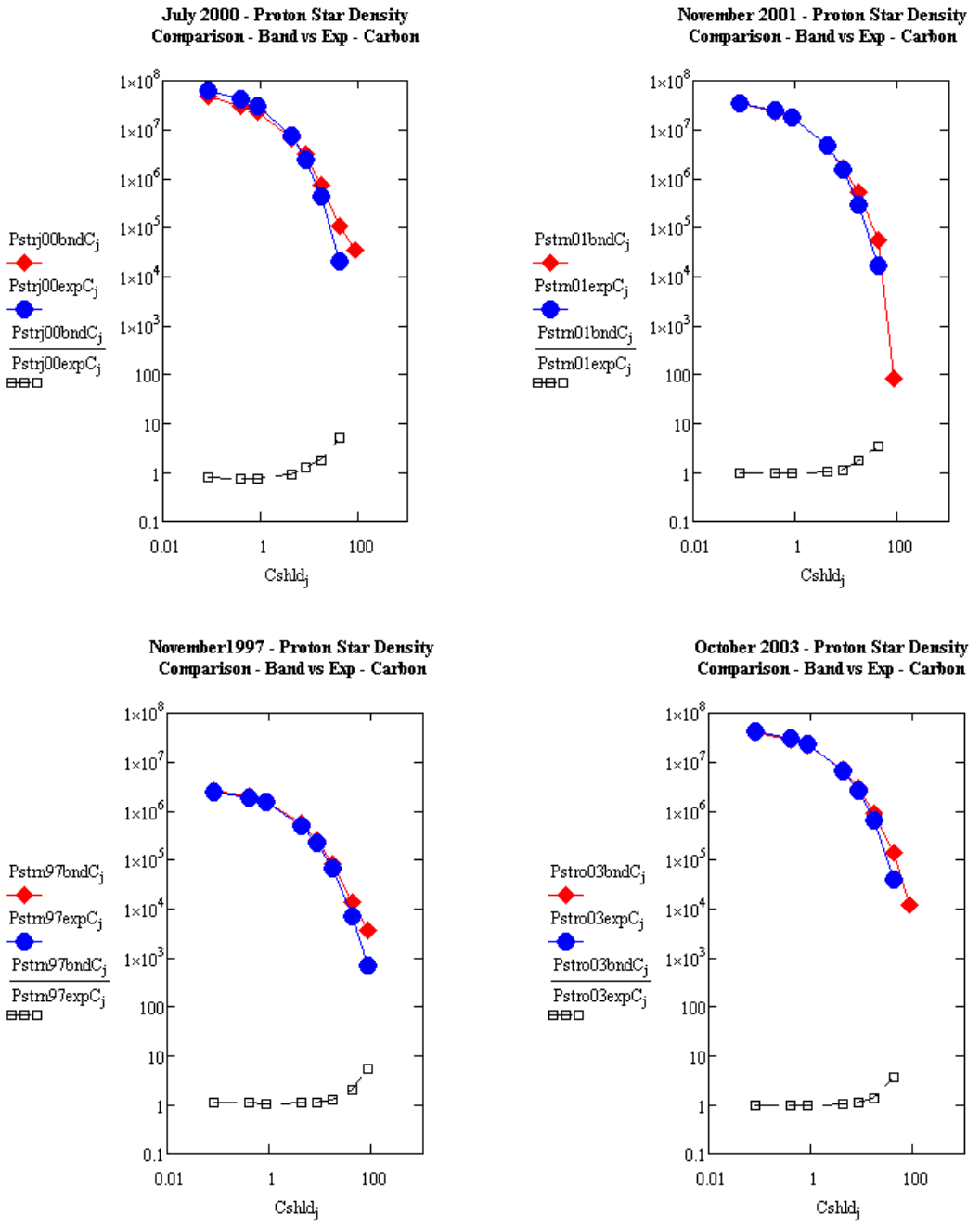


Figure 13. Proton star density, in number per cc (y axis, range 0.1 to 10^5), to the silicon detector shells as a function of shielding mass in g/cm^2 *titanium* (x axis, range 0.1 to 1 000) for each of the four particle events considered in this paper. Event star density resulting from Band (◆) and Exponential (●) event spectra is plotted as is the ratio [Band star density]/[Exponential star density] (□).

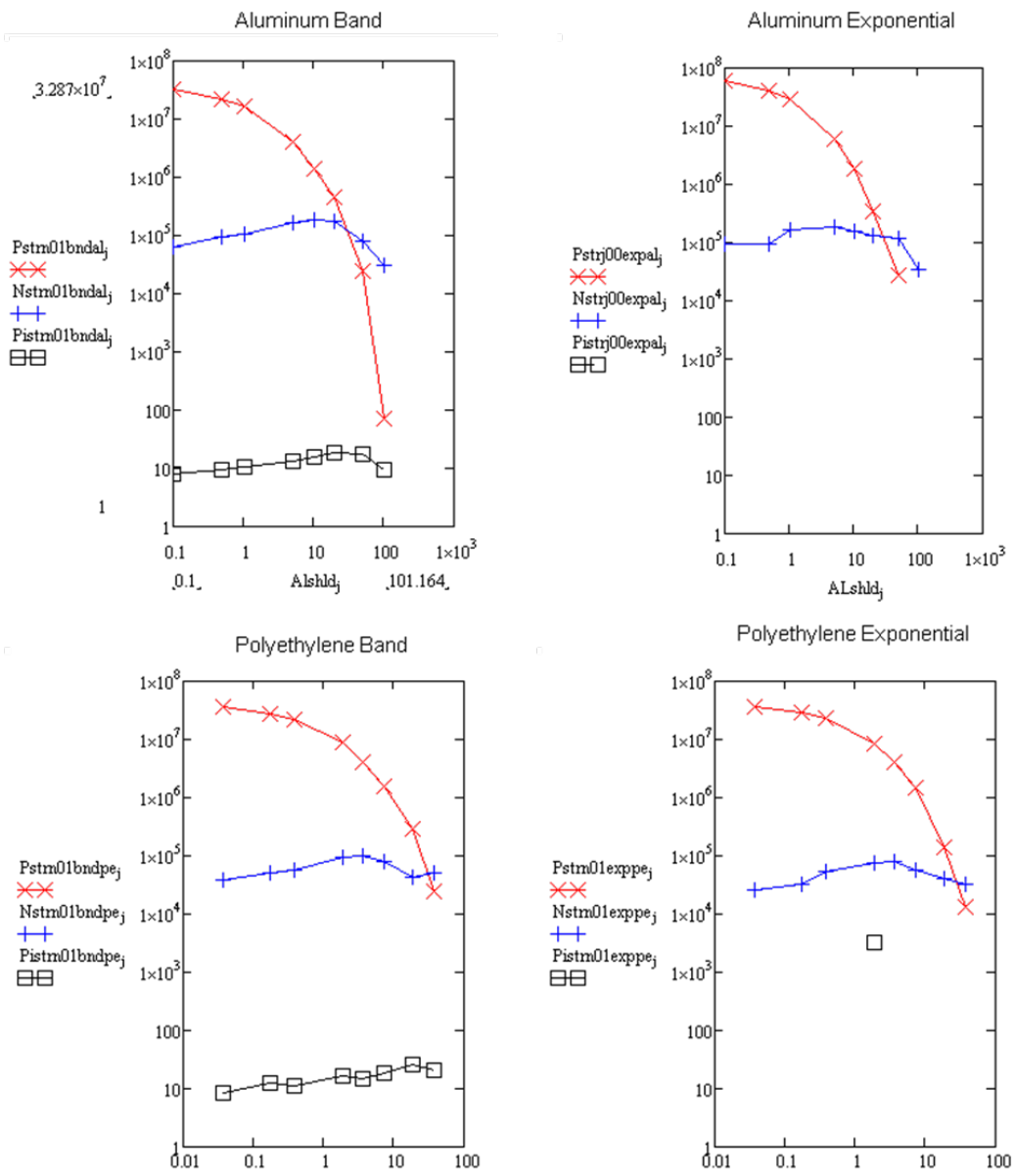


Figure 14. Proton, neutron, and pion star density, in number per cc (y axis, range 10 to 10^8), to the silicon detector shells as a function of aluminum or polyethylene shielding mass in g/cm^2. November 2001 SPE Band and Exponential event spectra. Proton star density (X), neutron star density (+), and pion star density (□).

5. Results and Discussion – Single-event Environment Rates

Calculated (estimated) and observed SPE SEU rates are compared in Table 3, along with the ratio (estimated rate)/(observed rate) for the three spacecraft/system and device combinations modeled here. The ratio (calculated rate)/(observed rate) ranges from 0.32 to 2.5, showing that the calculated and observed rates are within a factor of 3 of each other in all cases – a remarkably good agreement given the uncertainties in system device shielding mass and the use of a constant proton upset cross section estimated with the Petersen-Barak method[21]. Agreement between estimated and observed upset rates to within a "factor of a few" is generally viewed as acceptable for engineering design and verification purposes[27] and is better than the order-of-magnitude agreement often seen in the published literature[28-30].

The magnitude of the heavy ion contribution to solar particle SEU rates is highly variable[25,26]. The SPE heavy ions, helium through iron, are of low kinetic energy compared to galactic cosmic rays of the same atomic number and can be easily removed by relatively thin shielding. In some cases, heavy ions have contributed as much as 45% of the observed SPE SEU rates while in others no heavy ion contributions are detectable[26]. Hansen et al[25] have shown that, for Thuraya, the observed upset rate is a complex function not only of proton and heavy ion flux but also of particle kinetic energy spectra and device shielding environment. Based on published literature on the subject[25-30], it seems unlikely the heavy ion content of the SPEs modeled here could increase the calculated rates by more than a factor of 1.5 so that heavy ion effects do not affect our conclusion; ie, that the reasonable agreement between in-flight SPE SEU rates and rates estimated using the FLUKA-based approach reported here provides at least partial validation of the subject FLUKA modeling approach.

Table 3. A comparison of observed in-flight SPE SEU counts with estimates of SPE SEU counts calculated with FLUKA radiation transport code

Spacecraft/System and Device	Nov. 1997 SPE Upsets/bit	July 2000 SPE Upsets/bit	Nov. 2001 SPE Upsets/bit	Oct. 2003 SPE Upsets/bit
Cassini/Solid State Recorder DRAM 1) Observed upsets 2) Estimated upsets 3) Estimated Observed	1) 4.4×10^{-7} 2) 1.4×10^{-7} 3) 0.32	NA	NA	NA
SOHO/Solid State Recorder DRAM 1) Observed upsets 2) Estimated upsets 3) Estimated/Observed	1) 4.4×10^{-6} 2) 2.110^{-6} 3) 0.48	1) 4.7×10^{-5} 2) 2.1×10^{-5} 3) 0.4	NA	NA
Thuraya/DSP DRAM 1) Observed upsets 2) Estimated upsets 3) Estimated/Observed	NA	NA	1) 2.0×10^{-6} 2) 2.8×10^{-6} 3) 1.4	1) 1.5×10^{-6} 2) 3.8×10^{-6} 3) 2.5

6. Summary and Conclusions

The FLUKA radiation transport code has been successfully used to determine changes in the TID and SEE environments behind aluminum, polyethylene, carbon, and titanium shielding masses when the assumed form (Band or Exponential) of the SPE kinetic energy spectra is changed. For all particle event and shielding mass combinations, the following are found to be true: The differences in the TID environment and the SEE environment between the two SPE spectral forms are most pronounced when the shielding mass is greater than 10 g/cm^2 or less than 1 g/cm^2. Band and Exponential spectra produce nearly identical results between 1 and 10 g/cm^2. Direct comparison of SPE spectral forms revels that the Band form has higher particle flunece than the Exponential form at both low and high kinetic energies, while the two forms are nearly identical at intermediate kinetic energies. It is likely that TID and SEE are dominated by low-energy protons at low (< 1g/cm^2) shielding mass values and high-energy protons at high (> 10 g/cm^2) shielding mass values while intermediate mass protons dominate dose between 1 and 10 g/cm^2. Similar results were obtained using the HZETRN deterministic transport code in a simple two-dimensional slab geometry, as shown in the Appendix.

The usual atomic number dependence of shielding mass effectiveness was observed. For example, using the July 2000 event Band spectrum, the shielding mass, measured along the sphere radius, needed to reduce the event ionizing dose to 1 cGy or less in the concentric sphere configuration is 30 g/cm^2 polyethylene, 37 g/cm^2 carbon, 40 g/cm^2 aluminum, and 43 g/cm^2 titanium. Using the Exponential July 2000 event spectrum, the shielding mass needed to reduce the event ionizing dose to 1 cGy or less is 22 g/cm^2 polyethylene, 25 g/cm^2 carbon, 29 g/cm^2 aluminum, and 32 g/cm^2 titanium.

For particle kinetic energies >50 MeV, proton star density displayed a very different dose depth distribution than did neutron and pion star density. Proton star density decreased rapidly with increasing shielding mass and was often overtaken by neutron star density between 10 and 100 g/cm^2. Pion and neutron star density was nearly constant as

shielding mass increased, typically exhibiting a shallow maximum near 10 g/cm^2. In nearly all cases, the Exponential spectral form produced no pion stars at all – a result expected from the energetic threshold for pion production and the very small number of primary protons above that kinetic energy in the Exponential spectra. The Band and Exponential spectral forms produced comparable secondary neutron yields and plots of star density vs. shielding mass.

Calculation of the >50 MeV proton event fluence at various shielding mass values using the corresponding proton star density and the proton inelastic interaction length allowed estimation of SPE SEU counts for three spacecraft that are in reasonable agreement with the observed in-flight SPE SEU counts, thus at least partially confirming the validity of the FLUKA-based modeling process.

7. References

[1]Coffey VN, Minow JI, Blackwell WC Jr, Bruce MB, Howard JW. Using space weather variability in evaluating the radiation environment design specifications for NASA's Constellation Program. Paper presented at: American Geophysical Union, Fall Meeting 2007; December 10, 2007; San Francisco, Calif. Available at: ams.confex.com/ams/pdfpapers/134166.pdf. Accessed August 31, 2010.

[2]Reames DV. Solar energetic particle variations. *Adv Space Res.* 2004;34:381–390.

[3]Burrell MO, Wright JJ, Watts JW. *A Preliminary Report on Energetic Space Radiation and Dose Rate Analysis*. Washington, D.C.: NASA Headquarters; 1966. NASA-TM-53531. b) Malitson HH, Webber WR. A summary of solar cosmic ray events. In: *Solar Proton Manual*. Washington, D.C.: NASA Headquarters; 1963. NASA-TRR-169. c)Webber WR. *An Evaluation of the Radiation Hazard Due to Solar-Particle Events*. Seattle, Wash: AeroSpace Division, the Boeing Company; 1963. Boeing Report D2-90469.

[4]Tylka AJ, Dietrich WF. Proton spectra in ground-level enhanced (GLE) solar particle events. Paper presented at: Committee on Space Research (COSPAR); July 2008; Montreal, Canada. Paper D23-0003-08.

[5]Atwell W, Tylka A, Dietrich W, Badavi FF. Radiation exposure estimates for extremely large solar proton events. Paper presented at: Committee on Space Research (COSPAR); July 2008; Montreal, Canada. Paper F25-0027-08.

[6]Atwell W, Tylka A, Dietrich W. Radiation exposures form several ground level enhancements during the 23rd Solar cycle. Paper presented at: AIAA SPACE 2009 Conference; September 14-17, 2009; Pasadena, Calif. Paper AIAA-2009-6597.

[7]Battistoni G, Muraro S, Sala PR, et al. The FLUKA code: description and benchmarking, In: Albrow M, Raja R, eds. *Proceedings of the Hadronic Shower Simulation Workshop 2006 Fermilab*. September 6-8, 2006., *Am Inst Phys Conf Proc*. 2007;896;31-49.

[8]Ferrari A, Sala PR, Fasso A, Ranft J. FLUKA: a multi-particle transport code. Available at: http://www.slac.stanford.edu/cgi-wrap/getdoc/slac-r-773.pdf. Accessed September 1, 2010.

[9]The official FLUKA site. Available at: http://www.fluka.org/fluka.php. Accessed September 1, 2010.

[10]Neutron monitor network : fundamental research and applications. Available at: http://www.nmdb.eu/?q=node/138. Accessed September 1, 2010.

[11]University of Delaware Bartol Research Institute Neutron Monitor Program. Available at: http://neutronm.bartol.udel.edu/. Accessed September 1, 2010.

[12]Baker DN. The occurrence of operational anomalies in spacecraft and their relationship to space weather. *IEEE Trans Plasma Sci.* 2000;28(6);2007-2016.

[13]Dyer CS, Hunter K, Clucas S, Campbell A. Observation of the solar particle events of October and November 2003 from CREDO and MPTB. *IEEE Trans Nucl. Sci.* 2004:51(6)3388–3393.

[14]Bedingfield KL, Leach RD, and Alexander MB, eds. *Spacecraft System Failures and Anomalies Attributed to the Natural Space Environment*. Huntsville, Ala: NASA Marshall Space Flight Center; 1993. NASA Reference Publication 1390.

[15]Tylka AJ, Dietrich WF, Boberg PR, Smith EC, Adams JH Jr. Single event upsets caused by solar energetic heavy ions. *IEEE Trans Nucl Sci*. 1996:43(6):2758-2766.

[16]Parodi K, Paganetti H, Cascio E, et al. PET/CT imaging for treatment verification after proton therapy: a study with plastic phantoms and metallic implants. *Med Phys*. 2007:34:419-435.

[17]Autischer M, Beck P, Kindl P, Latocha M, Rollet S. Calibration and background measurements with a tissue equivalent proportional counter. *Radiat Prot Dosim*. 2007:125(1-4):429-432. Available at: http://rpd.oxfordjournals.org/content/125/1-4/429.full. Accessed September 1, 2010.

[18]Beck P, Wind M, Rollet S, et al. Microdosimetric GEANT4 and FLUKA Monte Carlo simulations and measurements of heavy ion irradiation of silicon and tissue. *IEEE Trans Nucl Sci*. 2006:53:3701-3706.

[19]FLUKA Online Manual. Available at: http://www.fluka.org/fluka.php?id=man_onl. Accessed September 1, 2010.

[20]Wilson JW, Cucinotta FA, Shinn JL, Simonsen LC. Overview of HZETRN and BRNTRN space radiation shielding codes. Paper presented at: Photonics for Space Environments IV; August 4-9, 1996; Denver, Colo. Available at http://www.tpub.com/content/nasa1996/NASA-96-pse4-jww/. Accessed September 1, 2010.

[21]Barak J, Reed, RA, LaBel, KA. On the figure of merit model for SEU rate calculations. *IEEE Trans Nucl Sci*. 1999;46(6);1504-1510.

[22]Groom DE. Atomic and nuclear properties of materials. *Journal of Physics G: Nuclear and Particle Physics – Review of Particle Physics*. 2006;33;106.

[23]Swift GM, Guertin S.M. In-flight observations of multiple-bit upset in DRAMs. *IEEE Trans Nucl Sci*. 2000;47(6);2386–2391.

[24]Harboe-Sorensen R, Daly E, Teston F, et al. Observation and analysis of single event effects on-board the SOHO satellite. *IEEE Trans Nucl Sci*. 2002;49(3);1345-1350.

[25]Hansen DL, Jobe K, Whittington J, Shoga M, Sunderland DA. Correlation of Prediction to on-orbit SEU performance for a commercial 0.25-µm CMOS SRAM. *IEEE Trans Nucl Sci*. 2007;54(6);2525-2533.

[26]Tylka AJ, Dietrich WF, Bobery PR. Probability distributions of high-energy solar-heavy-ion fluxes from IMP-8: 1973-1996. *IEEE Trans Nucl Sci*. 1997;44(6);2140–2149.

[27]Edmonds LD, Barnes CE, Scheick LZ. *An Introduction to Space Radiation Effects on Microelectronics*. Pasadena, Calif: NASA Jet Propulsion Laboratory, California Institute of Technology; 2000. JPL Publication 00-06.

[28]Petersen EL. Predictions and observations of SEU rates in space. *IEEE Trans Nucl Sci*. 1997;44(6);2174-2287.

[29]Petersen EL. The SEU figure of merit and proton upset rate calculations. *IEEE Trans Nucl Sci*. 1998;45(6);2550-2562.

[30]Reed RA, Kinnison J, Pickel JC, et al. Single-event effects ground testing and on-orbit rate prediction methods: the past, present, and future. *IEEE Trans Nucl Sci*. 2003;50(3);622-634.

Appendix

Figures App-1a and -1b, below, show the results of two-dimensional (slab target) HZETRN dose depth calculations for the band and exponential forms of the July 14, 2000 SPE over the shielding mass range 1 to 100 g/cm^2. As was observed for the FLUKA three-dimensional (spherical shell target) calculations, the Band and Exponential spectra produce nearly the same dose over the 1 to 10 g/cm^2 shielding mass range while the Band dose exceeds the Exponential dose over the 10 to 100 g/cm^2 shielding mass range.

Figures App-1c and -1d compare the three-dimensional FLUKA and two-dimensional HZETRN dose-depth results for the July 14, 2000 Band spectra. As expected, the two-dimensional HZETRN and three-dimensional FLUKA results are similar at low shielding mass and diverge at higher shielding mass where the three-dimensional effects of the shielding mass distribution function become more important.

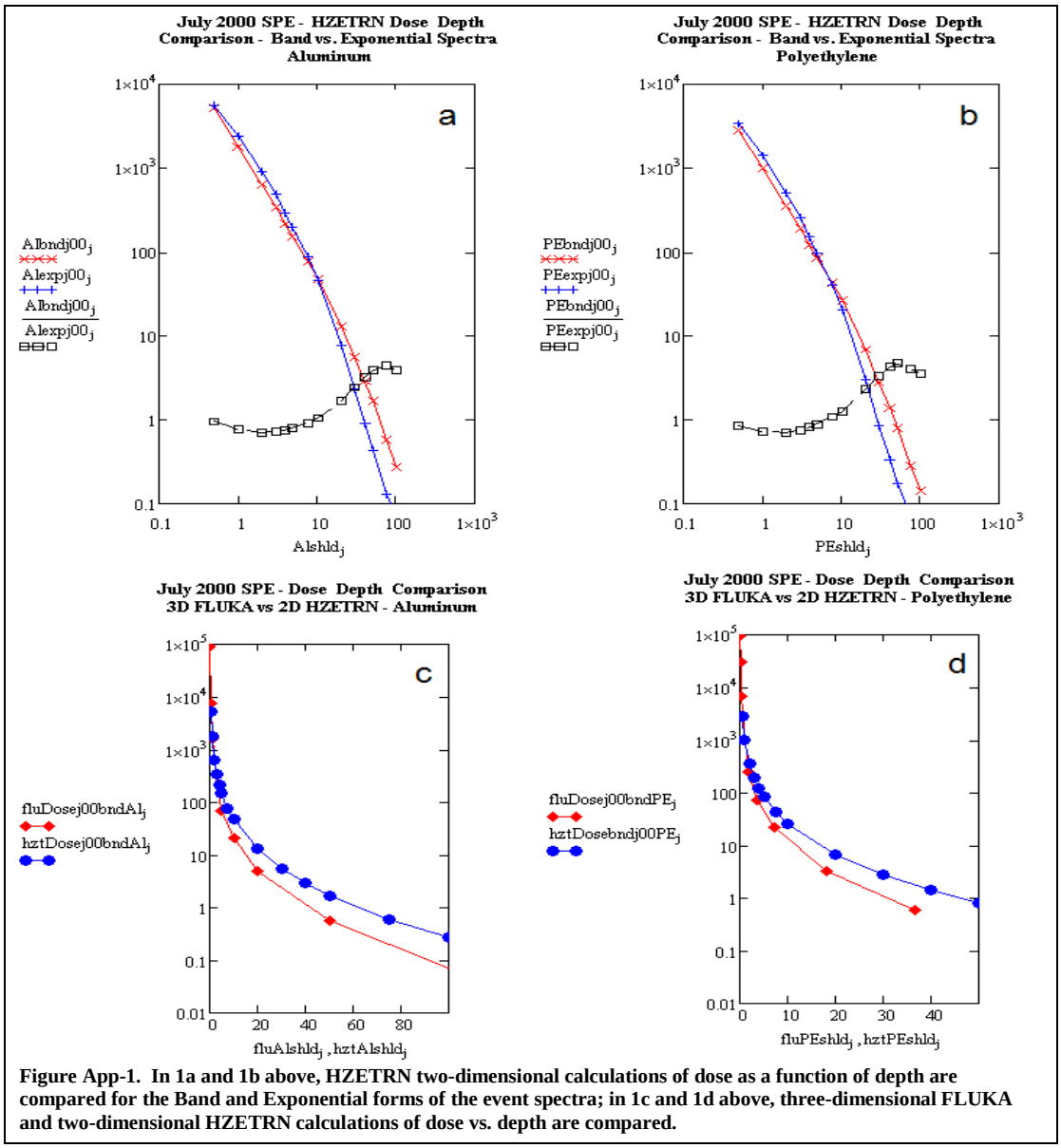


Figure App-1. In 1a and 1b above, HZETRN two-dimensional calculations of dose as a function of depth are compared for the Band and Exponential forms of the event spectra; in 1c and 1d above, three-dimensional FLUKA and two-dimensional HZETRN calculations of dose vs. depth are compared.

REPORT DOCUMENTATION PAGE			Form Approved OMB No. 0704-0188

Public reporting burden for this collection of information is estimated to average 1 hour per response, including the time for reviewing instructions, searching existing data sources, gathering and maintaining the data needed, and completing and reviewing the collection of information. Send comments regarding this burden estimate or any other aspect of this collection of information, including suggestions for reducing this burden, to Washington Headquarters Services, Directorate for Information Operations and Reports, 1215 Jefferson Davis Highway, Suite 1204, Arlington, VA 22202-4302, and to the Office of Management and Budget, Paperwork Reduction Project (0704-0188), Washington, DC 20503.

1. AGENCY USE ONLY *(Leave Blank)*	2. REPORT DATE	3. REPORT TYPE AND DATES COVERED
	September 2010	Technical Publication

4. TITLE AND SUBTITLE
Spacecraft Solar Particle Event (SPE) Shielding: Shielding Effectiveness as a Function of SPE Model as Determined with the FLUKA Radiation Transport Code

5. FUNDING NUMBERS

6. AUTHOR(S)
Steve Koontz*, William Atwell**, Brandon Reddell*, Kristina Rojdev*/***

7. PERFORMING ORGANIZATION NAME(S) AND ADDRESS(ES)
Lyndon B. Johnson Space Center
Houston, Texas 77058

8. PERFORMING ORGANIZATION REPORT NUMBERS
S-1079

9. SPONSORING/MONITORING AGENCY NAME(S) AND ADDRESS(ES)
National Aeronautics and Space Administration
Washington, DC 20546-0001

10. SPONSORING/MONITORING AGENCY REPORT NUMBER
TP-2010-216133

11. SUPPLEMENTARY NOTES
*NASA Johnson Space Center, Houston; **The Boeing Company, Boeing Research & Technology, Houston; ***PhD Student, University of Southern California, Los Angeles

12a. DISTRIBUTION/AVAILABILITY STATEMENT
Unclassified/Unlimited
Available from the NASA Center for AeroSpace Information (CASI)
7115 Standard
Hanover, MD 21076-1320 Category: 39

12b. DISTRIBUTION CODE

13. ABSTRACT *(Maximum 200 words)*

In this paper, we report the results of modeling and simulation studies in which the radiation transport code FLUKA (FLUktuierende KAskade) is used to determine the changes in total ionizing dose (TID) and single-event effect (SEE) environments behind aluminum, polyethylene, carbon, and titanium shielding masses when the assumed form (ie, Band or Exponential) of the solar particle event (SPE) kinetic energy spectra is changed. FLUKA simulations have fully three spatial dimensions with an isotropic particle flux incident on a concentric spherical shell shielding mass and detector structure. The effects are reported of both energetic primary protons penetrating the shield mass and secondary particle showers caused by energetic primary protons colliding with shielding mass nuclei. SPE heavy ion spectra are not addressed. Our results, in agreement with previous studies, show that use of the Exponential form of the event spectra can seriously underestimate spacecraft SPE TID and single-event environments in some, but not all, shielding mass cases.

14. SUBJECT TERMS	15. NUMBER OF PAGES	16. PRICE CODE
investigation; simulation; radiation transport; radiation dosage; radiation shielding; radiation spectra; particle interactions	34	

17. SECURITY CLASSIFICATION OF REPORT	18. SECURITY CLASSIFICATION OF THIS PAGE	19. SECURITY CLASSIFICATION OF ABSTRACT	20. LIMITATION OF ABSTRACT
Unclassified	Unclassified	Unclassified	Unlimited